Supplementary Notes for Continuous Visual Navigation with Ant-Inspired Memories

Gabriel Gattaux[1*], Antoine Wystrach[2], Julien R. Serres[1,3], Franck Ruffier[1]

[1*]Aix Marseille Univ, CNRS, ISM, Marseille, France.
[2]Univ Toulouse, CRCA, CBI, UMR CNRS-UPS 5169, Toulouse, France.
[3]Institut Universitaire de France, IUF, Paris, France.

*Corresponding author(s). E-mail(s): gabriel.gattaux@univ-amu.fr;

Supplementary note 1: Left and right familiarities with varying oscillation amplitude

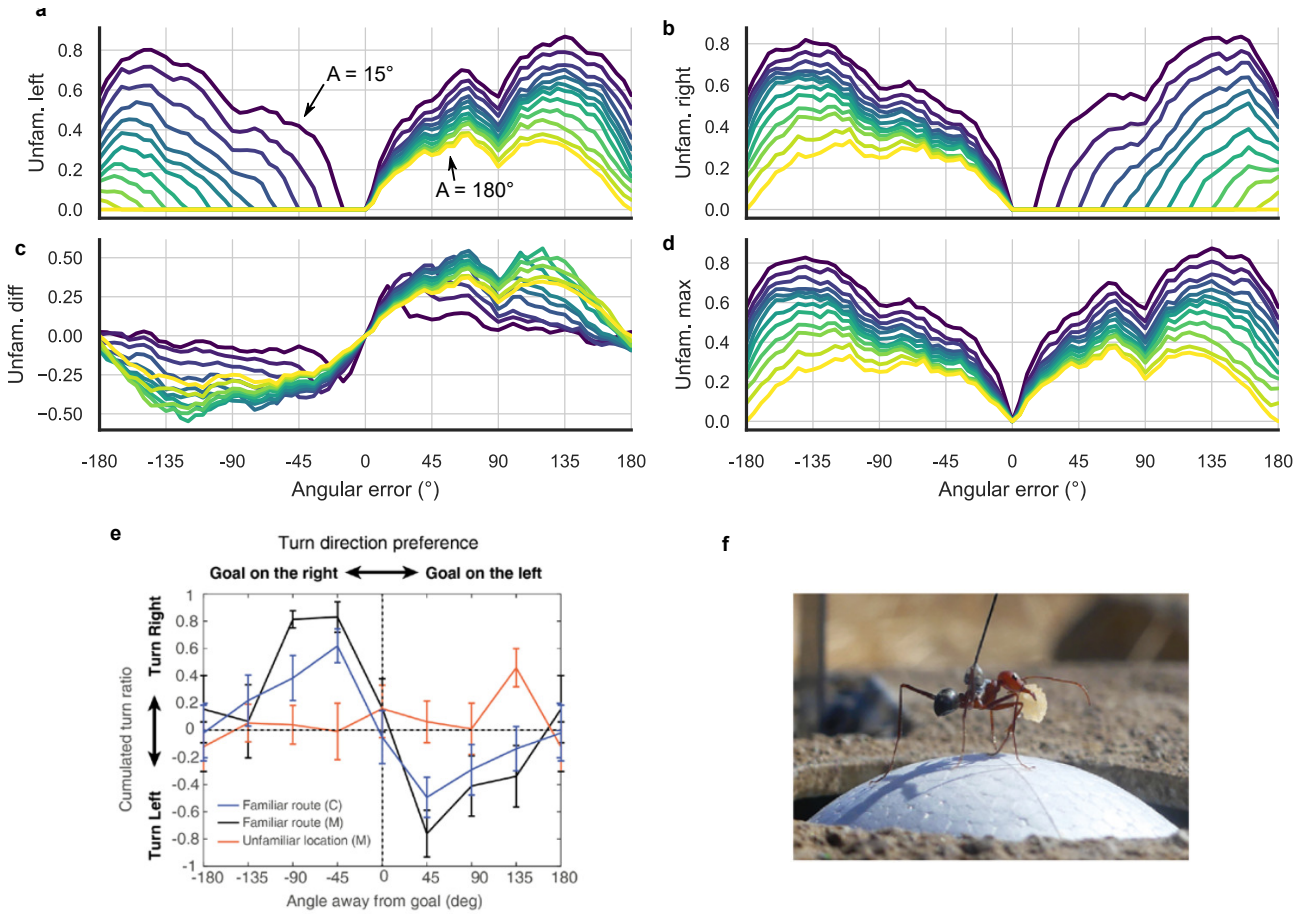

Fig. S1: **Indoor familiarity value relative to the oscillation amplitude and ants experiments**. The experimental setup was conducted indoors with artificial visual cues. **a** Familiarity from the left MBON. **b** Familiarity from the right MBON. **c** Differential familiarity. **d** Maximum familiarity. **e** Turn direction preference of various *Cataglyphis velox* (C) and *Myrmecia croslandi* (M) ants [1]. **f** A Cataglyphis ant carrying a cookie while moving on a ball [1].

To assess the self-supervised hypothesis, the images were captured and learned offline along a route (here indoor), and for each image, the familiarity (λ_L and λ_R) were computed for all orientation on the route from the two route MBONs, and plotted against the angular error (see supplementary Figs. S1a and S1b).

The familiarity were plotted for different oscillation amplitude during learning. Interestingly, we observed a similar pattern in the difference of familiarity (λ_{diff}) when the oscillation amplitude was approximately 45 degrees, resembling the turn direction preferences seen in ants [1] (see supplementary Figs. S1c, S1e and S1f).

Supplementary note 2: The advantages of several lateralized memories

The familiarity function when the visual compass is used – when only the direction of the route is learned in one MBON– resembles closely to the maximum familiarity of the route MBONs (see Fig. S1, S2a and S2b).

During visual compass methods [2], where one familiarity values was used, the agent had to navigate by minimizing the catchment area (area in the familairity function where the familiarity drop), and thus recover the route direction. However, since forced scanning in all direction is too much unnecessary calculation, gradient descent approach or klinokinesis were proposed as well [3, 4]. However, errors can occur when the catchment area contains local minima, as in indoor settings here (see Fig. S2d), revealed by the spatial derivative (along the angular error axis) of the familiarity value (See Figs. S2b and S2e). Therefore, the correct sign of the function within the catchment area appeared outdoors (See Fig. S2b) but is not clear indoor (See Fig. S2e), necessitating temporal filtering (in this case, a Savitzky-Golay filter with a window size of 21 inputs). A higher refreshing rate could be required to maintain an adequate control rate after filtering to keep this filtered derivative. Additionally, since the two catchment areas are not identical, the value of the derivative will not be similar, and therefore proportional gains must be fine-tuned for in different environments.

Interestingly, the raw difference between the two routes familiarity MBONs (see Figs. S2c and S2f) produced a function similar to the spatially filtered catchment area. This similarity was consistent across indoor and outdoor settings without the need for additional filtering. This demonstrates the importance of the learning in a lateralized manner, which enabled robust and consistent behavior in several environments without extensive tuning. These findings suggest that using the raw familiarity difference is well-suited for directly inputting into an autonomously controlled system, as it simplifies the process and eliminates the need for complex filtering mechanisms.

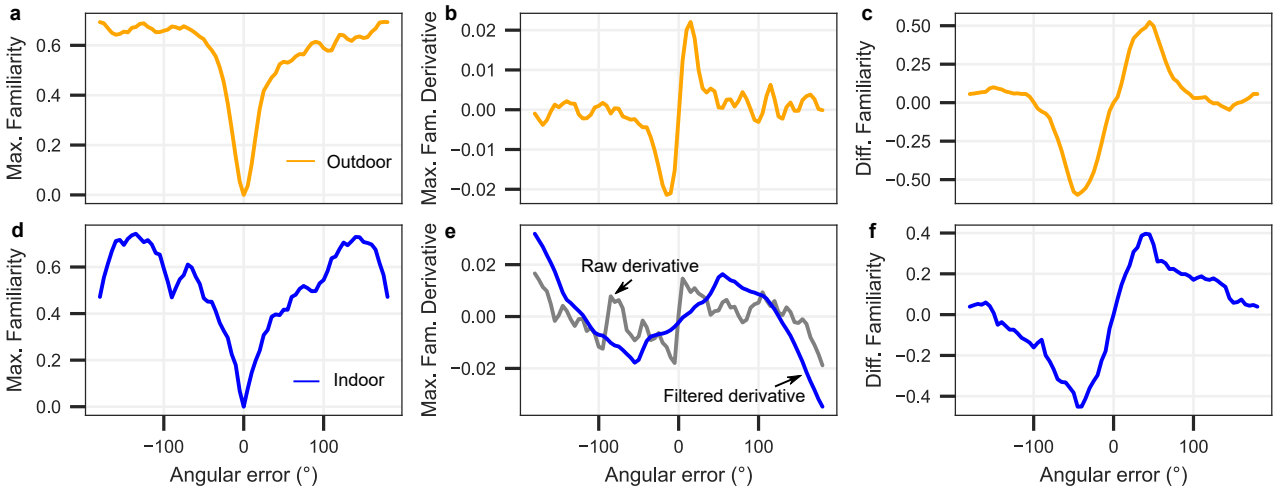

Fig. S2: **Comparison of familiarity derivative over angular error**. **a-c** Outdoor. **d-f** Indoor. **a,d** Maximum familiarity. **b,e** Spatial derivative of the maximum familiarity values. **c,f** Difference between left and right familiarities.

Supplementary note 3: Robot kinematic model in the Frenet frame

This note derives the simplified kinematic model of a car-like robot in the Frenet frame of reference and propose a control input. Unlike unicycle or differential drive robots, a car-like robot employs the Ackermann steering principle to prevent front-wheel slippage (see Fig. S3a). The initial configuration space of the car-like robot is described by $q = (x, y, \theta, \varphi)$, where (x, y) represents the position of point P_r (midpoint of the rear axle), θ is the robot's orientation, and φ is the steering angle defined at point P_a (midpoint of the front axle). The kinematic equations of the car-like robot are given by [5]:

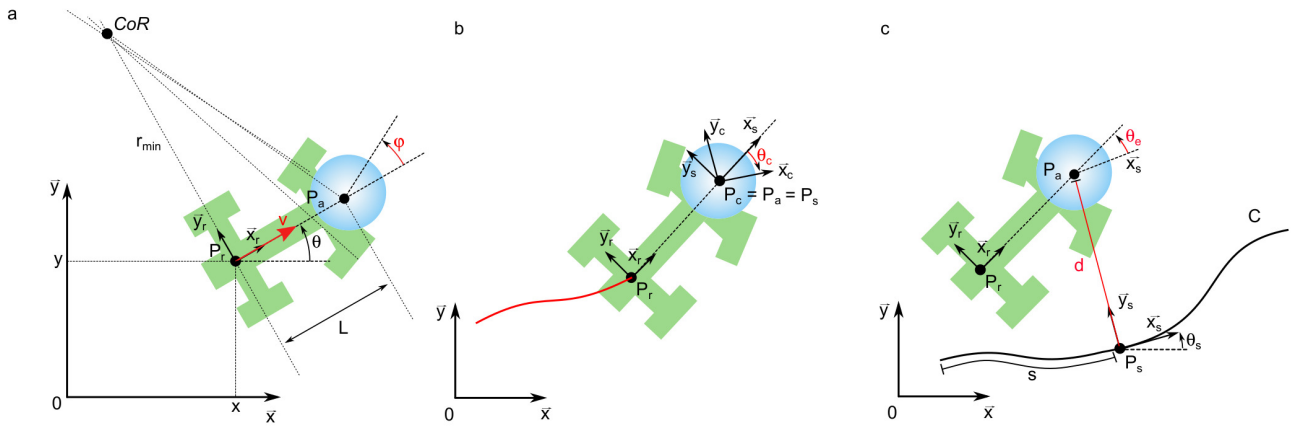

Fig. S3: **Car-like robot kinematics and frame. a** The configuration variables of a car like robot in a global frame of reference. **b** The camera frame relative to the robot frame while learning a route (in red) **c** The coordinate of the robot in the Frenet frame (dynamic local route point).

$$\dot{q} = \begin{bmatrix} \dot{x} \\ \dot{y} \\ \dot{\theta} \\ \dot{\varphi} \end{bmatrix} = \begin{bmatrix} cos(\theta) & 0 \\ sin(\theta) & 0 \\ \frac{tan(\varphi)}{L} & 0 \\ 0 & 1 \end{bmatrix} \begin{bmatrix} \nu \\ \omega \end{bmatrix}, \tag{1}$$

where v is the longitudinal velocity (See Fig. S3a), and ω is the steering rate ($\dot{\varphi}$). Assuming the steering rate ω_{max} is high enough to allow instantaneous steering angle changes, the model simplifies to $q = (x, y, \theta)$, resulting in:

$$\dot{q} = \begin{bmatrix} \dot{x} \\ \dot{y} \\ \dot{\theta} \end{bmatrix} = \begin{bmatrix} v \cdot \cos(\theta) \\ v \cdot \sin(\theta) \\ v \cdot \frac{\tan(\varphi)}{L} \end{bmatrix}, \tag{2}$$

In practice, the throttle input τ (ranging from 0 to 1) controls the (Pulse Width Modulation) PWM values sent to the motors, thus modifying velocity v. For simplicity, we assume v is a function of throttle, $v = f(\tau, v_{max})$, where v_{max} is the maximum speed at full throttle in a straight line. Furthermore non-holonomic constraints prevent the car from moving sideways, resulting in:

$$\dot{x} \cdot \sin(\theta) - \dot{y} \cdot \cos(\theta) = 0 \tag{3}$$

indicating that the robot can only turn if it has a non-zero linear speed.

To address the route-following problem, the Frenet-Serret frame is used as a reference [6]. Let C be a curve with an attached frame $F_s = P_s, \vec{x_s}, \vec{y_s}$, where $\vec{x_s}$ is tangent to C. The motion of P_a with respect to F_s is described by the states $q = (s, d, \theta_e)$, where s is the distance traveled along C, d is the lateral error (distance from P_a to C), and θ_e is the angular error between the robot's orientation and the tangent of the dynamic local route (See Fig. S3). Thus,

$$\theta_e = \theta - \theta_s \tag{4}$$

where θ_s is the dynamic local route orientation in the global frame (See Fig. S3). The motion equations for $\dot{\theta}_e$ are derived from (2) and (4), assuming a momentarily constant route orientation ($\dot{\theta}_s = 0$). This assumption [7] simplifies the calculation of motion equations by assuming that the route orientation does not vary significantly over a small time interval. Thus,

$$\begin{aligned} \dot{\theta_e} &= \dot{\theta} \\ &= v \cdot \frac{tan(\varphi)}{L} \end{aligned} \tag{5}$$

Using the transport theorem, we derive the full set of motion equations in the Frenet frame (as in [6] but simplified here) :

$$\dot{q} = \begin{bmatrix} \dot{s} \\ \dot{d} \\ \dot{\theta_e} \end{bmatrix} = \begin{bmatrix} v \cdot (\cos\theta_e - \tan\varphi \sin\theta_e) \\ v \cdot (\sin\theta_e + \tan\varphi \cos\theta_e) \\ v \cdot \frac{\tan\varphi}{L} \end{bmatrix}, \tag{6}$$

The angular error must remain below 90° to avoid losing control due to perpendicular alignment (tangent effect). Based on the empirical results in the main paper, we proposed that the model stayed valid within a 2-meter lateral corridor around the learned route and a 45° angular error, in relation with the learning oscillation amplitude A, leading to:

$$D = \{(d, \theta_e) \mid |d| < 1 \text{ m and } |\theta_e| < 45°\} \tag{7}$$

Within this domain, we proposed a proportional relationship between the familiarity difference λ_{diff} and angular error θ_e thanks to the observed linearity in the main paper:

$$K_{diff} \cdot \lambda_{diff} = -\theta_e \tag{8}$$

where K_{diff} is a negative gain. Then, we propose the following control input U:

$$U = \begin{bmatrix} v \\ \varphi \end{bmatrix} = \begin{bmatrix} M \cdot K_v \cdot sat(1 - \lambda_{max}) \\ M \cdot K_\varphi \cdot \lambda_{diff} \end{bmatrix}, \tag{9}$$

Supplementary note 4 : Lyapunov stability analysis

To evaluate the stability of the overall system, we introduce a Lyapunov function [8] that is positive definite. The function $V(d, \theta_e)$ is constructed such that it is positive definite ($V(d, \theta_e) \geq 0$) for all $d \neq 0$ and $\theta_e \neq 0$, and it equals zero only when $d = 0$ and $\theta_e = 0$. The proposed Lyapunov function is:

$$V(d, \theta_e) = \frac{1}{2}\left(d^2 + \theta_e^2\right) \tag{10}$$

For the system to be considered asymptotically stable, the derivative of this Lyapunov function, $V(\dot{d}, \theta_e)$, must be negative for all $d \neq 0$ and $\theta_e \neq 0$, and zero when $d = 0$ and $\theta_e = 0$. This implies that the system not only remains near equilibrium but eventually converges to it . The derivative of the Lyapunov function is:

$$\dot{V}(d, \theta_e) = d\dot{d} + \theta_e\dot{\theta_e} \tag{11}$$

Then, by integrating the model' equation 2 to the derivative Lyapunov function 11 and the control actions equation 9 for φ (we set $v = 1$ for simplification, knowing that v will be always positive or negative but without change on a route-following task) and fixed the motivation state $M = 1$, we get :

$$\begin{aligned} \dot{V}(d, \theta_e) &= dv(\sin\theta_e + \tan\varphi\cos\theta_e) + \theta_e\frac{\tan\varphi}{L} \\ &= d(\sin\theta_e + \tan(K_\varphi\lambda_{diff})\cos\theta_e) \\ &+ \theta_e\frac{\tan(K_\varphi\lambda_{diff})}{L} \end{aligned} \tag{12}$$

Then, we apply the proposition depicted in equation 8, we obtain :

$$\begin{aligned} \dot{V}(d, \theta_e) &= d(\sin\theta_e + \tan -\theta_e\cos\theta_e) + \theta_e \cdot \frac{\tan -\theta_e}{L} \\ &= d(\sin\theta_e + \frac{\sin -\theta_e}{\cos -\theta_e}\cos\theta_e) + \theta_e \cdot \frac{\tan -\theta_e}{L} \\ &= d(\sin\theta_e + \sin -\theta_e) + \theta_e\frac{\tan -\theta_e}{L} \\ &= d(\sin\theta_e - \sin\theta_e) + \theta_e\frac{\tan -\theta_e}{L} \\ &= -\theta_e \cdot \frac{\tan\theta_e}{L} \end{aligned} \tag{13}$$

The θ_e sign will cancel itself out if it is within plus or minus 90 degrees, due to the tangent function and the similar sign of λ_{diff} relative to θ_e. Consequently, the negative sign of the resulting derivative of the Lyapunov function in (13) satisfies the conditions $\dot{V}(d, \theta_e) < 0$ for all $d \neq 0$ and $\theta_e \neq 0$, and $\dot{V}(0, 0) = 0$ within the domain limits specified in (7). Therefore, the system is proven to be asymptotically stable within these conditions.

Supplementary note 5 : Extended experimental data

The overview of the left and right familiarities, with the difference, the maximum, the linear and angular velocities are depicted in Fig. S4 and in the Table S7. Furthermore, the crash which occurred during kidnapped robot and during occlusion are shown in Fig. S5, with two other indoor route following experiments not shown in the main

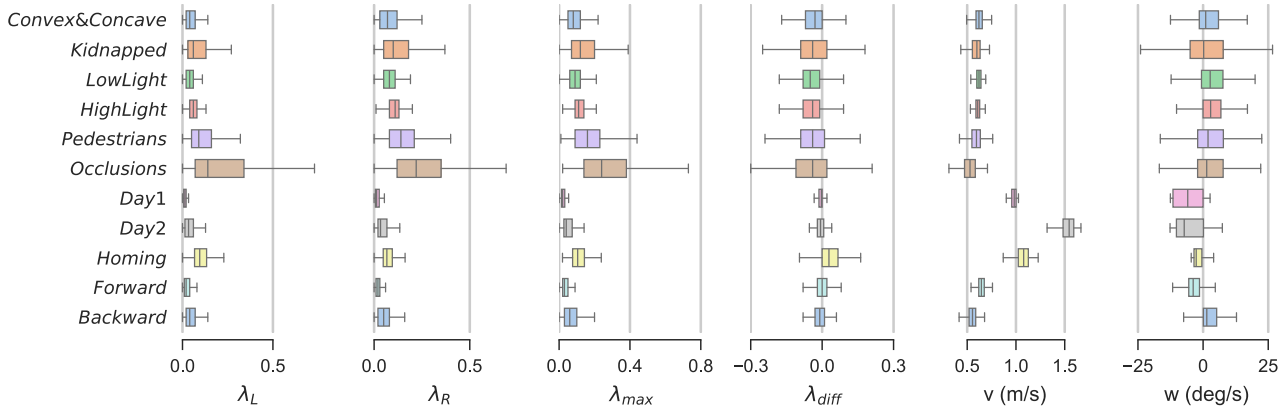

Fig. S4: **Detailed variables during experiments**. Boxplots representing the left and right familiarity (λ_L and λ_R), the difference (λ_{diff}), the maximum λ_{max}, the linear speed (v), and the angular speed (w) for each experiment.

paper but taken into account in *Convex&Concave* statistics. The poses learned during shuttling and homing experiments are also shown in Fig. S6 with the endpoint familiarity plotted in the background.

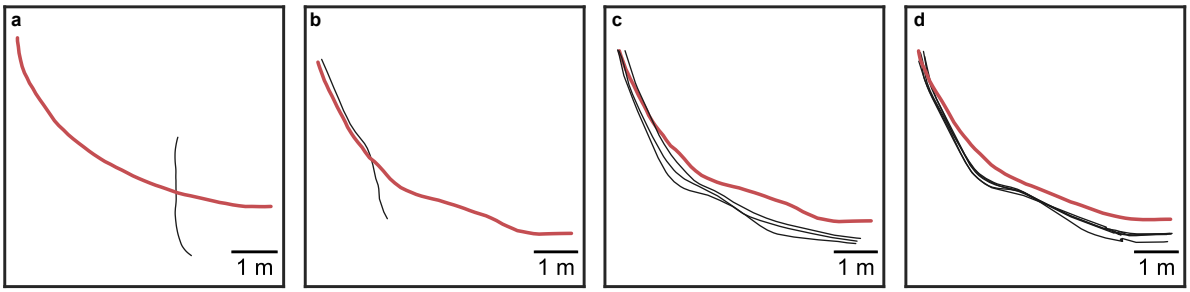

Fig. S5: **Supplementary trajectories. a** The crash during the kidnapped robot experiment. **b** Crash during dynamic occlusion. **c** Three trajectories, in normal conditions before pedestrians experiment, grouped in *Convex&Concave*. **d** Five trajectories in normal conditions grouped in *Convex&Concave* cases.

Table S7: Summary statistics by experiment.

Experiment	**Lateral Error (m)**		**Angular Error (°)**		**Diff. Familiarity**	
ID	**Median**	**MAD**	**Median**	**MAD**	**Median**	**MAD**
Convex&Concave	0.22	0.10	3.45	2.25	-0.03	0.04
Kidnapped	0.27	0.14	6.46	4.19	-0.04	0.05
Low Light	0.24	0.08	3.81	2.09	-0.05	0.03
High Light	0.20	0.06	3.88	2.33	-0.04	0.03
Pedestrians	0.27	0.15	4.05	2.82	-0.04	0.05
Occlusions	0.23	0.13	4.72	3.29	-0.04	0.06
Day1	0.40	0.13	5.77	2.79	-0.00	0.01
Day2	1.32	0.47	6.19	3.22	-0.01	0.01
Homing	0.89	0.54	6.28	4.16	0.03	0.04
Forward	0.11	0.04	1.26	0.84	0.00	0.02
Backward	0.19	0.08	2.73	2.16	-0.01	0.02
Experiment	**Max Familiarity**		**Angular Speed (°/s)**		**Linear Speed (m/s)**	
ID	**Median**	**MAD**	**Median**	**MAD**	**Median**	**MAD**
Convex&Concave	0.08	0.03	1.00	3.46	0.62	0.03
Kidnapped	0.12	0.06	0.22	6.32	0.60	0.04
Low Light	0.09	0.03	2.72	4.01	0.62	0.02
High Light	0.11	0.03	2.89	3.24	0.61	0.02
Pedestrians	0.16	0.07	1.89	4.60	0.59	0.04
Occlusions	0.24	0.11	1.39	4.75	0.53	0.06
Day1	0.02	0.01	-5.90	5.86	0.98	0.02
Day2	0.04	0.02	-7.25	3.67	1.55	0.05
Homing	0.10	0.03	-2.65	0.94	1.08	0.05
Forward	0.03	0.01	-3.80	1.97	0.65	0.03
Backward	0.06	0.03	1.42	1.91	0.55	0.03

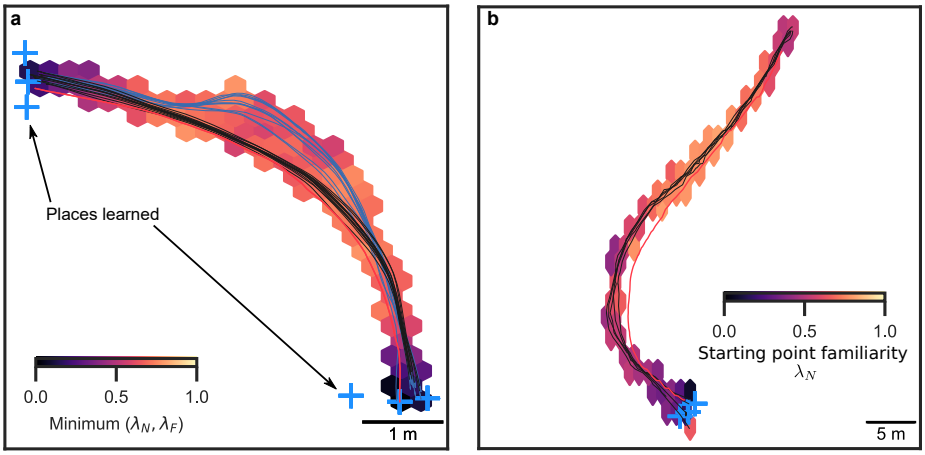

Fig. S6: **Endpoint learning in shuttling and homing experiments. a** Shuttling experiments: the background shows the minimum familiarity between the two endpoint's MBONs (Nest and Feeder), with blue crosses indicating the learned poses. **b** Homing experiments: Nest MBONs familiarity in background and trajectories in foreground

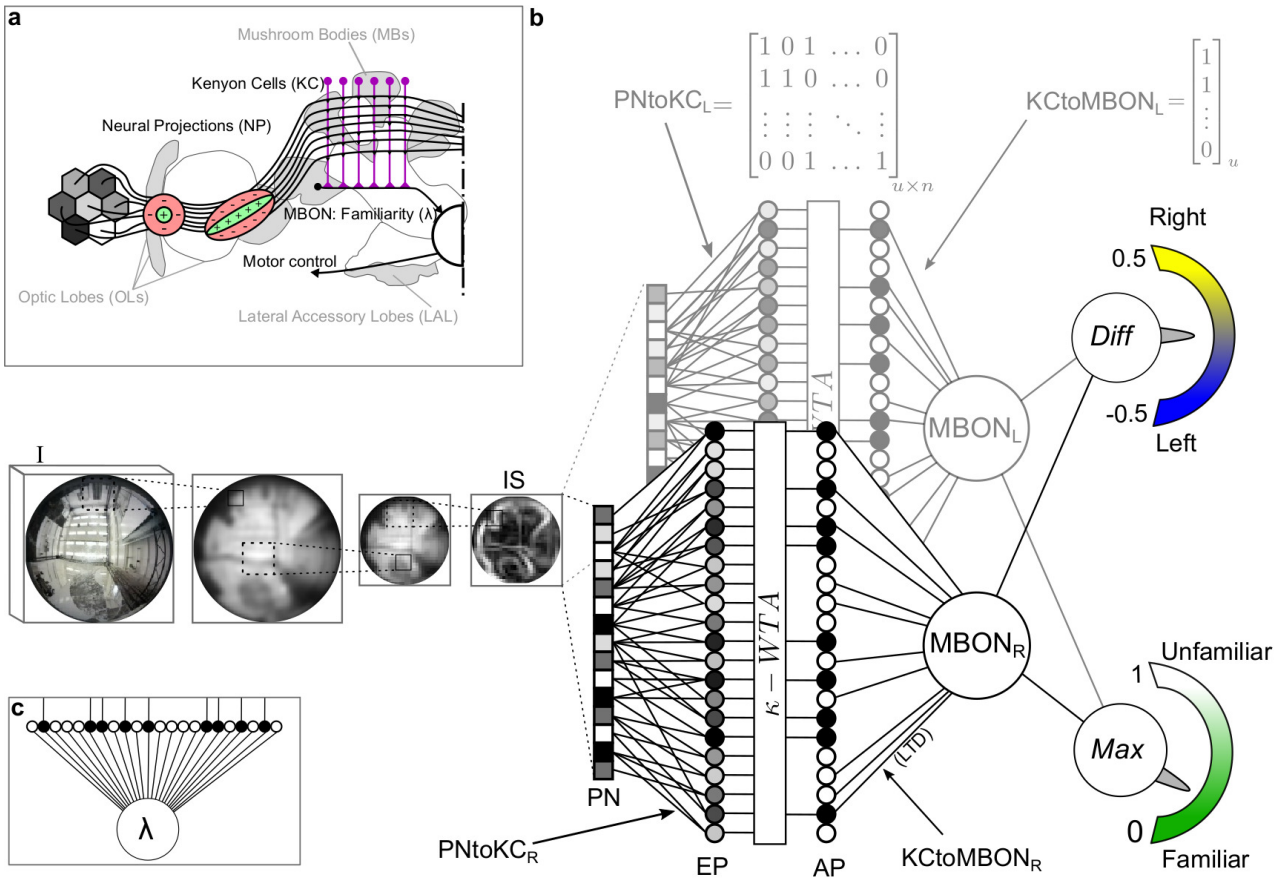

Fig. S7: **Detailed mushroom body neural network for route following. a** Biological representation of the neural network. **b** Detailed representation with the two Mushroom Bodies Output Neurons during exploitation. **c** The KCtoMBON synaptic weight matrix before learning

References

[1] Wystrach, A., Le Moël, F., Clement, L. & Schwarz, S. A lateralised design for the interaction of visual memories and heading representations in navigating ants. *BioRxiv* (2020).

[2] Gattaux, G., Vimbert, R., Wystrach, A., Serres, J. R. & Ruffier, F. Antcar: Simple Route Following Task with Ants-Inspired Vision and Neural Model. *HAL archive* (2023).

[3] Möller, R. & Vardy, A. Local visual homing by matched-filter descent in image distances. *Biological Cybernetics* **95**, 413–430 (2006).

[4] Kodzhabashev, A. & Mangan, M. Wilson, S. P., Verschure, P. F., Mura, A. & Prescott, T. J. (eds) *Route Following Without Scanning*. (eds Wilson, S. P., Verschure, P. F., Mura, A. & Prescott, T. J.) *Biomimetic and Biohybrid Systems*, Vol. 9222, 199–210 (Springer International Publishing, Cham, 2015).

[5] Lynch, K. *Modern Robotics* (Cambridge University Press, 2017).

[6] Morin, P. & Samson, C. Motion control of wheeled mobile robots. *Springer handbook of robotics* **1**, 799–826 (2008).

[7] Applonie, R. & Jin, Y.-F. A novel steering control for car-like robots based on lyapunov stability. *2019 American Control Conference (ACC)* 2396–2401 (2019).

[8] Lyapunov, A. M. The general problem of the stability of motion. *International journal of control* **55**, 531–534 (1992).